COMPUTATIONAL AND EXPERIMENTAL STUDY OF ENERGETIC MATERIALS IN A COUNTERFLOW MICROGRAVITY ENVIRONMENT

NASA Final Report
NASA Grant NCC3-718

M. D. Smooke
Yale University

T. P. Parr and D. M. Hanson-Parr
Naval Air Warfare Center China Lake

R. A. Yetter and G. Risha
The Pennsylvania State University

ABSTRACT

Counterflow diffusion flames are studied for various fuels flowing against decomposition products from solid ammonium perchlorate (AP) pellets in order to obtain fundamental understanding of composite propellant flame structure and chemistry. We illustrate this approach through a combined experimental and numerical study of a fuel mixture consisting of C_2H_4, CO + H_2, and C_2H_2 + C_2H_4 flowing against solid AP. For these particular AP-fuel systems, the resulting flame zone simulates the various flame structures that are expected to exist between reaction products from AP crystals and a hydrocarbon binder. As in all our experimental studies, quantitative species and temperature profiles have been measured between the fuel exit and AP surface. Species measured included CN, NH, NO, OH, N_2, O_2, CO_2, H_2, CO, HCl, and H_2O. Temperature was measured using a thermocouple at the exit, spontaneous Raman scattering measurements throughout the flame, OH rotational population distributions, and NO vibrational population distributions. The burning rate of AP was also measured as a function of strain rate, given by the separation distance between the AP surface and the gaseous hydrocarbon fuel tube exit plane. This distance was nominally set at 5 mm, although studies have been performed for variations in separation distance. The measured 12 scalars are compared with predictions from a detailed gas-phase kinetics model consisting of 86 species and 531 reactions. Model predictions are found to be in good agreement with experiment and illustrate the type of kinetic features that may be expected to occur in propellants when AP particle size distributions are varied. Furthermore, the results constitute the continued development of a necessary database and validation of a comprehensive model for studying more complex AP-solid fuel systems in microgravity. Exploratory studies have also been performed with liquid and solid fuels at normal gravity. Because of melting (and hence dripping) and deep thermal wave penetration into the liquid, these experiments were found feasible, but not useful for obtaining quantitative data. Microgravity experiments are needed to eliminate the dripping and boiling phenomena of these systems at normal gravity.

Microgravity tests in the NASA Glenn 2.2 second drop tower were performed (1) to demonstrate the feasibility of performing propellant experiments using the NASA Glenn microgravity facilities, (2) to develop the operational procedures for safe handling of the energetic materials and deposal of their toxic combustion by-products and (3) to obtain initial measurements of the AP burning rate and flame structure under microgravity conditions. Experiments were conducted on the CH_4/AP system previously studied at normal gravity using a modified design of the counterflow burner and a NASA Glenn Pig Rig, i.e., one of the existing drop rigs for general-purpose usage. In these experiments, the AP burning rate was measured directly with a linear variable differential transducer (LVDT) and video imaging of the flame structure was recorded. Ignition was achieved by hot wires stretched across the AP surfaces. Initial drop tower combustion data show that with the same burner separation distance and flow conditions of the normal gravity experiments, the AP burning rate is approximately a factor of two lower. This difference is likely a result of radiation effects, but further tests with longer test times need to be conducted to verify that steady state conditions were achieved under microgravity conditions.

INTRODUCTION

The potential to 1) increase specific impulse, muzzle velocity, and payload mass, as well as 2) assess the safety and reliability of systems containing propellants or explosives that are subjected to normal and abnormal environments, is highly dependent upon the ability to formulate and to model new and existing energetic materials. Systems of this type could be monopropellants or energetic composites comprising oxidizer particles of different sizes, which are randomly imbedded, for example, in a thermoplastic elastomeric binder. The development of advanced propellants employing new nitramines and energetic binders requires a more sophisticated approach than the conventional methods of testing a matrix of ingredients to arrive at a formulation empirically. The latter approach is too costly and time-consuming for the large matrix of nitramine/binder combinations.

In the present research, we have developed a combined experimental and computational program that focuses on the prediction of micro combustion parameters like flame structure, temperature profile, heat release, and species concentrations as well as global parameters such as burn rate and pressure exponent for development of a comprehensive propellant combustion model that may eventually be used for design and optimization of propellant formulations as well as study of their storage and disposal. We studied propellant ingredient combinations through a systematic approach using a counterflow diffusion flame configuration, which separates the fuel and oxidizer and extends the reaction zones spatially, allowing diagnostics to measure quantitative species and temperature profiles while simplifying the fluid flow of the numerical simulations allowing the program to concentrate on propellant kinetics.

In a typical counterflow diffusion flame experiment two laminar plug flow jets, one of fuel and one of oxidizer, are directed at each other so they impinge in the middle of the domain. Properly designed, this configuration leads to one-dimensional flames that can be modeled with the lower CPU demand of 1D codes. In addition, the experimenter has complete

control over many flame parameters including fuel chemistry, fuel thermal properties, flame strain rate, etc. In our case the oxidizer side is not a jet but a solid pellet of ammonium perchlorate (AP) (Fig. 1). AP does not normally self deflagrate at pressures below about 200 PSIA (depending on purity), but in the counterflow configuration, AP flames are observed to be self-sustained even at 1 atm, with nearly perfect planar multi-flame structures.

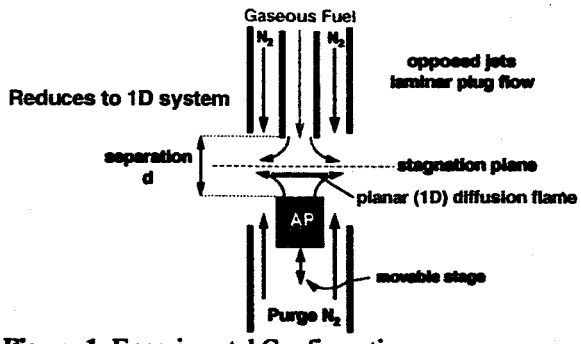

Figure 1. Experimental Configuration.

In the current program, we have studied the structure of AP/methane, AP/ethylene, AP/carbon monoxide and hydrogen flames and AP/acetylene and ethylene flames [1-6]. These flame structures represent the fundamental building blocks of more complex hydrocarbon based binder systems. For example, ethylene is an important decomposition product of hydroxyl-terminated polybutadiene (HTPB), while methane, carbon monoxide and hydrogen are important sub-mechanisms of ethylene combustion. Furthermore, by selective variations in the fuel composition, we have been able to mimic particular regions of the flame region and the effect of macroscopic variations of the propellant formulation such as the AP particle size. Diagnostics applied to these flames include thermocouple temperature profiles, spatially and spectrally resolved chemiluminescent emission profiles, Planar Laser Induced Fluorescence (PLIF) 2D imaging of CN, NH, NO, OH, OH rotational temperature, and PAH, line of sight absolute calibration of PLIF profiles using UV-visible absorption imaging, planar 2D imaging of soot via Laser Induced incandescence (LII) , and 1D profiles of N_2, O_2, CH_4, H_2O, and HCl via point Raman scattering. Utilizing recent developments in hydrocarbon, chlorine, NO_x, N_xH_y, and AP kinetics, a detailed transport, finite rate chemistry system was formulated for the temperature, velocity and species mass fractions of the combined flame system.

AP/C_2H_4 GASEOUS FUEL DIFFUSION FLAME STUDIES

We investigated the modeling of counterflow diffusion flames in which the products of AP combustion are counter flowed against an ethylene fuel stream. The two-dimensional problem can be reduced to a one-dimensional boundary value problem along the stagnation point streamline through the introduction of a similarity transformation. By utilizing recent developments in hydrocarbon, chlorine, NOx and AP kinetics, we can formulate a detailed transport, finite rate chemistry system for the temperature, velocity and species mass fractions of the combined flame system. A detailed soot model is included which can predict soot volume fractions as a function of the strain rate and the fuel mole fraction. We compared the results of this model with a series of experimental measurements in which the temperature was measured with radiation-corrected thermocouples and OH rotational population distribution, several important species were measured with PLIF, UV-visible

absorption, and Raman spectroscopies, and the soot volume fraction was measured with laser-induced incandescence and visible absorption spectroscopy (see Figs. 2 and 3).

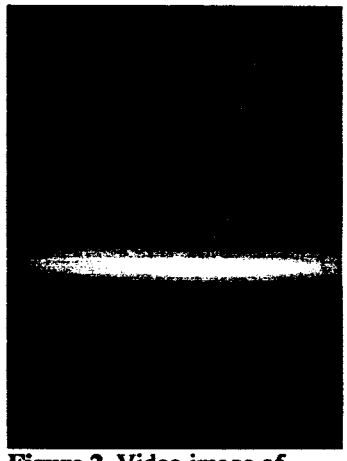

Figure 2. Video image of AP/ethylene counterflow flame.

A comparison of the computed and absolute soot volume fraction is illustrated in Fig 3. The figure indicates that the soot is localized in a very thin region (1 mm) in the fuel rich portion of the flame. This is consistent with the visual observations reported in [7]. Excellent agreement is obtained for the spatial locations of the computed and measured soot volume fractions as well as the absolute peak heights (0.41 ppm versus 0.43 ppm). Relative spatial distributions for the separate processes of surface growth, soot inception, and oxidation as determined from the model indicate that the soot oxidation rates observable in this flame are attributable to super-equilibrium OH concentrations, consistent with our previous study [8]. Results not illustrated here indicate that the peak soot volume fraction is extremely sensitive to the strain rate of the system. An order of magnitude reduction in the peak soot volume fraction can be obtained by a moderate increase of the strain rate. This is attributed in part to 1) the variation in peak mole fractions of key growth species such as acetylene and benzene as a function of the strain rate, 2) the temperature dependence of the inception and surface growth processes as a function of the strain rate and 3) the significant decrease in residence time as the strain rate increases.

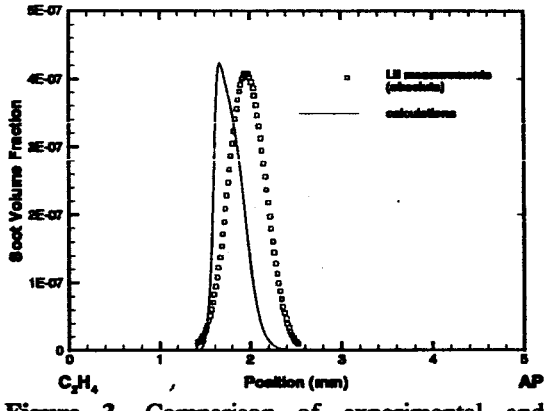

Figure 3. Comparison of experimental and computational soot volume fraction for the AP/ethylene counterflow flame.

AP/($CO+H_2$) GASEOUS FUEL DIFFUSION FLAME STUDIES

Most composite propellants based on AP contain a bimodal or trimodal particle size distribution of AP. A typical formulation would contain 85% solids (AP) with 15% binder (e.g., HTPB). The AP would consist of a mixture of coarse and fine AP particles (e.g., 62% 200 μm and 38% 25 μm). In our prior studies, we used methane and ethylene as representatives of the HTPB decomposition gases that would burn with the fine AP. Here, the fuel was a mixture of H_2 and CO in the ratio of 52 to 48 mole percent, respectively. This simulates the chemistry of the combustion products from the binder (HTPB) and fine AP fraction of a composite propellant, which go on to react in a diffusion flame with the large diameter AP fraction. In the formulation example given, the neat AP flame (above large diameter AP crystals) would be 1377K, the fine AP/binder flame would be 1162K, and the final flame between the decomposition products from the large AP and the AP/binder flame products would be 2645K.

Details of the experimental techniques and numerical procedures can be found in our previous papers. Figures 4a and 4b show representative OH and NO PLIF images. Note the clean image above the OH PLIF due to the lack of fuel decomposition products such as PAH and/or soot LII, as was seen for AP/CH_4, and especially AP/C_2H_4 counterflow flames. Color imaging (Fig. 4c) shows two distinct regions for the AP/(H_2+CO) flame. This compares with four colored flame regions in the methane AP case (Fig. 4d). Note also that the AP pellet burns relatively flat and the gas flames are very flat. Both images show the same thin orangish flame near the AP surface and a thicker light blue flame above it (which spatially corresponds to OH radicals in the PLIF image). The bright purple bluish flame above the OH* seen in the methane case is missing for AP/(H_2+CO). The bluish color was chemiluminescence from CN* and NH* radicals which are missing from the hydrogen/carbon monoxide AP flame. There is a top reddish "flame" towards the fuel side for AP/methane, not well shown in the exposure case for Fig. 4d, which correlates with soot volume fraction and is undoubtedly faint black body emission from soot. The AP/(H_2+CO) flame produces no soot.

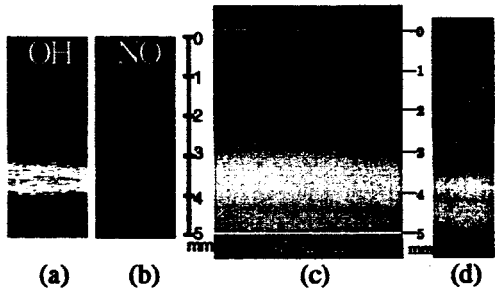

Figure 4. AP/(H_2+CO) counterflow diffusion flame PLIF images, 5 mm separation between the AP surface and fuel exit. The AP is at the bottom and fuel at the top. (a) OH PLIF. (b) NO PLIF. (c) Close-up view of the AP/(H_2+CO) counterflow diffusion flame and (d) AP/CH_4 counterflow diffusion flame for comparison.

The experimental temperature profile is shown in Fig. 5. The Stokes/Anti-Stokes Raman results match the OH rotational temperature quite well. Also shown are temperatures obtained from total density (from total Raman Stokes signal); these match the other measurements as well. Temperatures from fitting NO vibrational spectra, shown in Fig. 5, also match. The calculated temperature, NO, OH and NH profiles are shown Fig. 6. In all the plots, the measured scalars are compared with the model predictions. With the exception of NO on the fuel rich side, model predictions and experiment are generally in good agreement. The NO profile predicted in the AP/CH_4 flame distinctively showed the sharp change in slope near 2.8 mm, which is absent from the prediction shown in Fig. 6. However, compared to the experimental data, the model indicates NO to be reduced at a faster rate in the fuel rich regions. Species profiles of CO, H_2, HCl, H_2O, CO_2, N2, and O_2, obtained from spontaneous Raman measurements and compared with numerical data. Model predictions are in good agreement, with the exception of CO_2, for which the experimental results were lower than the predictions.

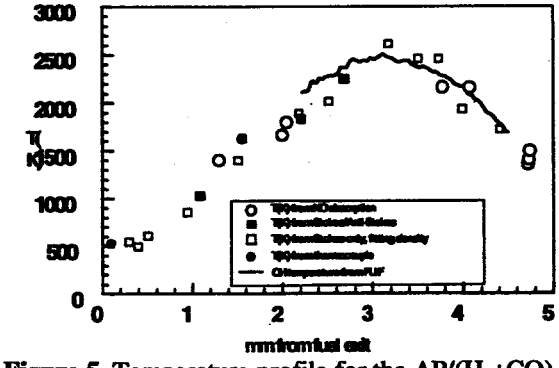

Figure 5. Temperature profile for the AP/(H_2+CO) counterflow diffusion flame with a 5 mm separation.

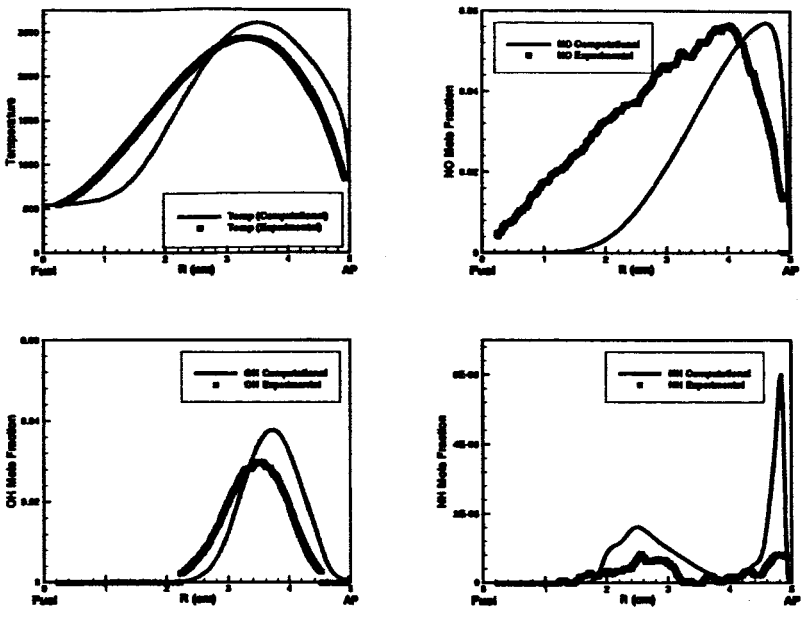

Figure 6. Comparison of experimental NO, OH and NH species profiles and the temperature with modeling results.

AP/(C_2H_2+C_2H_4) GASEOUS FUEL DIFFUSION FLAME STUDIES

Counterflow diffusion flame experiments and modeling results are presented for a fuel mixture consisting of N_2, C_2H_2 and C_2H_4 flowing against decomposition products from a solid AP pellet. The flame zone simulates the diffusion flame structure that is expected to exist between reaction products from AP crystals and a hydrocarbon binder. Quantitative species and temperature profiles have been measured for one strain rate, given by a separation of 5 mm, between the fuel exit and the AP surface. Species measured include C_2H_2, C_2H_4, N_2, CN, NH, OH, CH, C_2, NO, NO_2, O_2, CO_2, H_2, CO, HCl, H_2O, and soot volume fraction. Temperature was measured using a combination of a thermocouple at the fuel exit and other selected locations, spontaneous Raman scattering measurements throughout the flame, NO vibrational populations, and OH rotationalpopulation distributions. The burning rate of the AP was also measured for this flame's strain rate. The measured eighteen scalars are compared with predictions from a detailed gas-phase kinetics model consisting of 105 species and 660 reactions. Model predictions are found to be in good agreement with experiment and illustrate the type of kinetic features that may be expected to occur in propellants when AP particles burn with the decomposition products of a polymeric binder. The model predicts an AP decomposition flame above the AP surface, followed by an (acetylene-ethylene)/AP-products diffusion flame, in agreement with experimental observations of the OH profile and the excited state CH. Both flame structures lie to the AP side of the stagnation plane. The AP/(N_2+C_2H_2+C_2H_4) system is remarkably rich in structure. Color imaging shows four distinct flame regions (right panel in Fig. 7) that are similar to those in the AP/CH4 counterflow flame (left panel in Fig. 7). Near the AP surface is an orange region containing the burnt gases of the AP

self-deflagration flame, which has an extremely short standoff distance. The second region that is light blue in color indicates where OH radicals first start to appear. This is followed by a third zone that is purple in color and contains the primary diffusion flame with high radical concentrations. Finally, as one moves towards the fuel jet, a bright yellowish region is visible which correlates with the soot volume fraction. The AP/(H_2+CO) flame (middle panel in Fig. 7), however, illustrates only two regions, i.e., the AP decomposition flame and the primary (H_2+CO)/AP-products diffusion flame. The bright purple bluish flame (chemiluminescence from CN^* and NH^* radicals) above the OH^* seen in the ethylene-acetylene case is missing for the AP/(H_2+CO) flame as is the sooting region. (In the AP/CH_4 case the lens used on the color camera passed UV, such as OH emission, and the camera may react to this by showing some blue exposure. The AP/(H_2+CO) experiments used a glass lens that didn't pass UV so the same flame shows as a salmon color.)

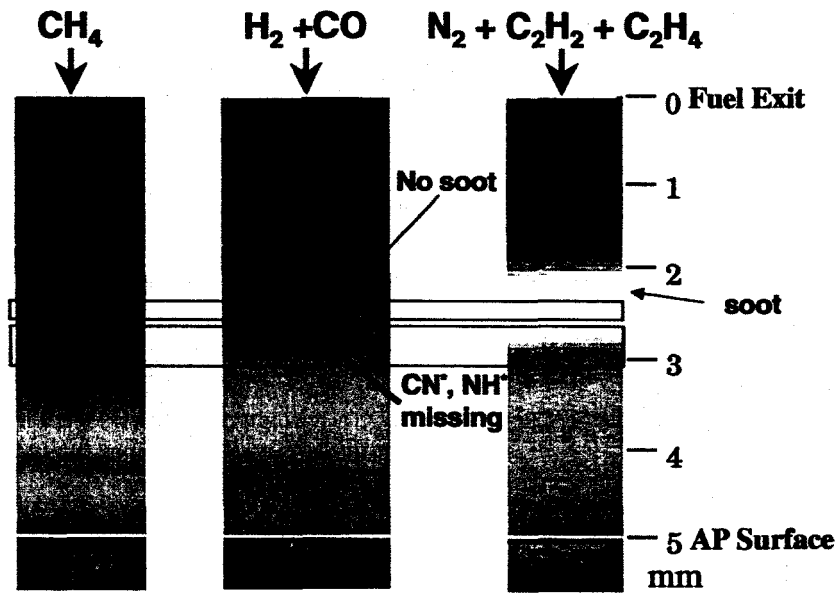

Figure 7. Video images of AP/CH_4 (left panel), AP/(H_2+CO) (middle panel) and AP/(N_2+ C_2H_2+C_2H_4) (left panel) counterflow diffusion flames.

For PLIF, each profile was taken down the centerline of the corresponding image, averaging over a horizontal distance small enough so that any slight surface irregularity did not impact the profile width. The temperature profile is shown in Fig. 8. Filled circles and open squares are from Raman Stokes (density) and Stokes/Anti-Stokes (ratio) measurements, open circles are from radiation-corrected thermocouples, and triangles are from fitting NO absorption. The Stokes/Anti-Stokes Raman results match the OH rotational temperature (solid line) quite well. The fuel exit temperature was approximately 332K measured using a thermocouple. The other thermocouple temperature measurements are shown in Fig. 8 as open circles. The temperature curve obtained from the model fits the data quite well from the AP surface up to the region of the stagnation plane, but diverges somewhat on the fuel side of the flame. Initially, we believed that this divergence was due to the fact that the model assumes plug flow at the burner (i.e., no radial velocity component) with the similarity variable equal to zero while the experiment may not be able to maintain strict plug flow conditions. The discrepancy caused by this velocity profile

would show up, not only in the temperature, but also in all the species profiles seen on the fuel side.

All of the modeling studies have been conducted with specification of the gas-phase speciation at the AP surface or at the fuel tube exit. We have studied several condensed phase reaction mechanisms for AP decomposition in the literature, and currently, none of these mechanisms is capable of predicting the gas-phase speciation measured at the AP surface. These mechanisms have generally been postulated from empirical evidence. Clearly, significant research, both experimental and theoretical, is required at the molecular level to develop our understanding and knowledge base of condensed phase processes.

AP COUNTERFLOW EXPERIMENTS WITH SOLID AND LIQUID FUELS

Many solid propellant binders and some oxidizers have liquid layers when they burn. In order to study realistic binders in simple flow geometries, some exploratory experiments were performed with condensed phase fuels and/or binders. In essence, these experiments are important because they change the complexity of the fuel boundary condition in a well-controlled manner. For example, choosing methanol as the fuel simply adds a vaporization process at the fuel boundary in the model without the need for condensed phase chemistry and decomposition. Methanol chemistry in the gas-phase is also important because it introduces OH radicals into the fuel flow with well-known gas phase kinetics. Hydroxyl radicals play a significant role in HTPB decomposition as well as in the decomposition of other solid fuels such as polyethylene glycol (PEG). PEG is a solid fuel that melts, and could be envisioned as an intermediate solid fuel to study in a hierarchical approach to building a HTPB decomposition mechanism just as we have used in developing gas phase mechanisms for realistic binders. Figure 9 shows AP burning with two different fuels; PEG and liquid methanol. For the PEG experiments, low regression rates led to very deep thermal profiles, which created a liquid layer present over a large spatial extent. For both fuels, extremely complex fluid dynamics were generated in the liquid due to the present of convective mass and heat transport resulting from subsurface phase transformation. Large-scale bubbles, particularly

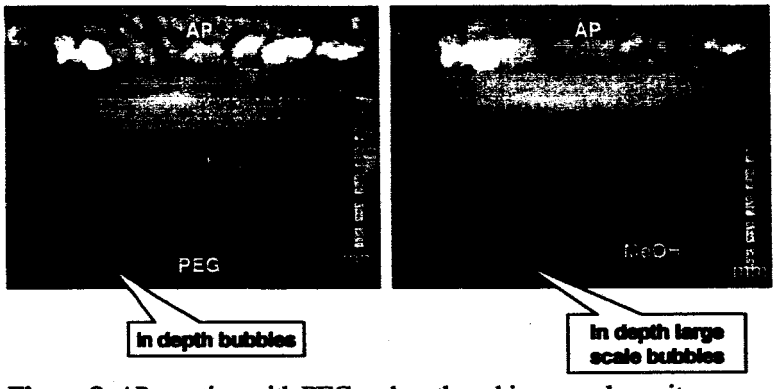

Figure 9. AP reacting with PEG and methanol in normal gravity.

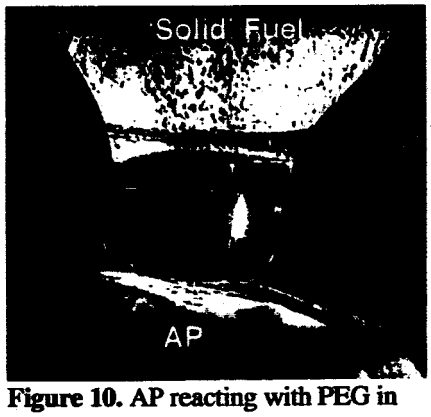

Figure 10. AP reacting with PEG in normal gravity.

noticeable in the case of methanol, and a poorly defined surface prevented the fuel side boundary condition from being well defined for modeling calculations and hence prohibited the collection of quantitative data. However, it is interesting to note that the gas-phase flame structure was stable and exhibited interesting chemical reaction zones as in the previously studied gaseous hydrocarbon flames.

Figure 10 shows the result of combusting AP again with PEG, but with the solid fuel and AP reversed with regards to the direction of gravity. Under these conditions, the PEG melted and dripped onto the AP surface preventing formation of the liquid pool as illustrated in Fig. 9. These results are encouraging and suggest that microgravity experiments should enable the collection of quantitative data for model development.

MICROGRAVITY STUDIES

Although all of our detailed studies have been performed in a 1-g environment, they have provided us with significant experience in the operation of counterflow solid AP – gaseous hydrocarbon flames. The modeling has enabled us to build the foundation chemistry with which to examine systems that are more complex. Our goal has been to study solid oxidizer – solid fuel counterflow systems. Because of melt layer dripping from the solid oxidizer or solid fuel surfaces, as shown above, and the effects of buoyancy on the flame structure, these systems cannot be studied in a 1-g environment. By operating under microgravity conditions, the length scales will be increased and the gravitational forces suppressed on melting binders such that increased resolution of both major and minor species will be possible thus reducing the demands placed on both the computational and

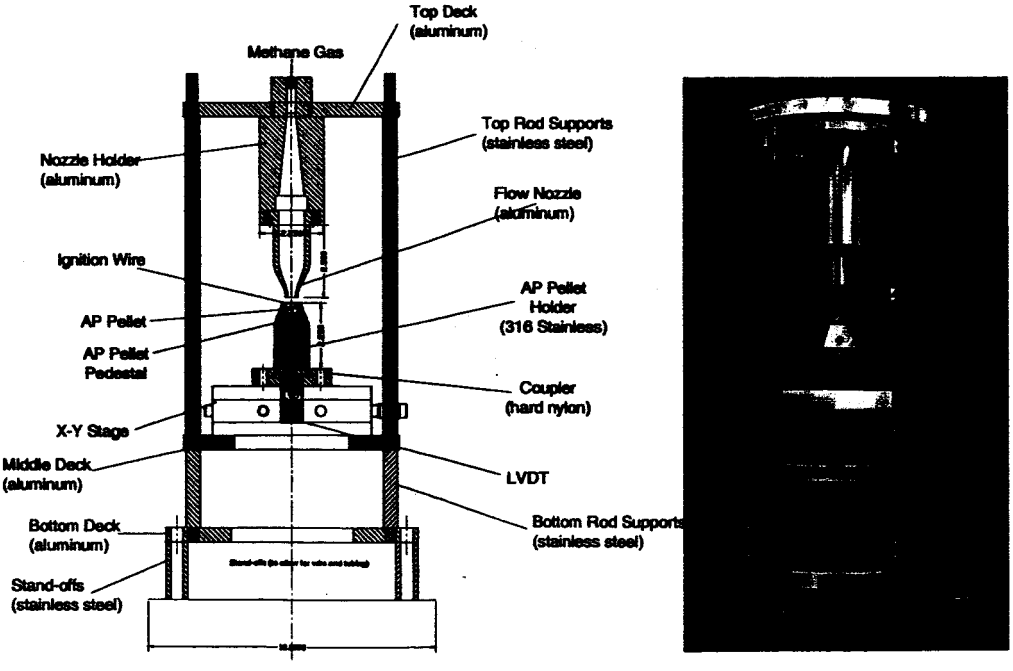

Figure 11. Schematic and photograph of the AP pellet assembly.

diagnostic tools. We have designed and initiated fabrication of a test rig for parabolic flight experiments. Because of significant safety requirements and our initial desire to maximize the number of scalars measured, the design and fabrication of this system has required several modifications.

As an intermediate step towards the parabolic flight experiments, microgravity tests in the NASA Glenn 2.2 second drop tower were performed (1) to develop the operational procedures for safe handling of the energetic materials and deposal of the toxic combustion by-products and (2) to obtain initial measurements of the AP burning rate and flame structure under microgravity conditions. Experiments were conducted on the CH_4/AP system previously studied at normal gravity using a modified design of the counterflow burner and a NASA Glenn Pig Rig, i.e., one of the existing drop rigs for general usage. In these experiments, the AP burning rate was measured directly with a LVDT and video imaging of the flame structure was recorded. Ignition was achieved by resistively heating a fine wire stretched across the AP surface.

For the microgravity version of the burner assembly (Fig. 11), the pellet was attached to an insulated pedestal, which was in direct contact with a high-precision LVDT. As the AP pellet pyrolyzed, the LVDT tracked axial location of the bottom surface of the pellet as it decomposed. The AP pellet was spring loaded in the pellet holder and held in place at the holder exit by a fine-wire permanently positioned across the external surface of the pellet to keep the top surface of the pellet stationary as the AP was consumed. The fine wire also acted as the ignition source. Ignition was achieved by continuously turning on and off power to the wire with a predetermined rate and duration. Normal gravity ignition experiments were conducted to determine the optimal duty cycle and heating period, which for the 24 V power supply on the test rig occurred with a 2.5% duty cycle and 3 second duration. The AP surface was also maintained at a predetermined distance below the exit plane of the methane nozzle so that the separation distance remained constant during an experiment (5 mm was chosen for these experiments). Figure 12 shows the burner assembly mounted in the test chamber from above and the Pig Rig ready to be lifted to the drop floor of the tower for a microgravity experiment.

Figure 12. The burner assembly in the combustion chamber of Pig Rig 4 and Pig Rig 4 ready for a drop test.

Prior to an experiment, the test chamber was prepared by (1) loading a single pellet into the burner, (2) inserting the burner into the test chamber of the Pig Rig, and (3) filling a methane storage tank to a pressure sufficient for a single drop experiment. The methane

flow rate for an experiment was preset using an OMEGA mass flow meter mounted on the test rig to a value of 0.86 LPM. The test chamber was evacuated and purged with nitrogen gas. After two cycles of evacuation and filling, the chamber was filled to atmospheric pressure with nitrogen. During the entire experiment, the test chamber was sealed. Since there is no exhaust from the test chamber during the experiment, the reactants undergo a constant volume combustion process.

Data were collected during an experiment using an on-board computer, which utilized a customized program written using Ttools software. The computer also served to control the automated sequence of operations during a drop test. In addition to monitoring the axial position of the AP pellet during an experiment, a pressure transducer was used to measure the instantaneous chamber pressure, a high-precision mass flow meter was used to record the gaseous methane flow rate, and a video camera was used to record the combustion event. All except the video signal were recorded by the onboard data acquisition system and downloaded for post-test processing and interpretation. The sampling rate of data acquisition was approximately 200 Hz. The video signal was transmitted out of the PIG Rig via a fiber optic to a stationary VCR or digital recorder located on the 8th floor of the drop tower. Six electrical lines were passed in and out of the combustion chamber: 1) power (2 lines) and output signal (2 lines) of the LVDT requiring four existing feedthroughs and 2) input leads (2 lines) requiring two feedthroughs, which handle significant current, for the ignition wire. The AP pellet assembly wiring diagram is given in Appendix A. In addition to the electrical feedthroughs, a gas feedthrough was required in order to supply gaseous methane to the reaction zone inside of the test chamber. A rigidly mounted stainless steel supply line was connected (inside the test chamber) from the CH_4 feedthrough (located at the bottom of the test chamber) to the top injection assembly.

Once the system integrity was verified by activating the indicator lamp mounted on the Pig Rig, the data acquisition (DAQ) system was armed and ready for drop. Immediately after releasing the Pig Rig package, the interlock circuitry was activated and the on-board computer began acquiring data and initiated a sequence of operations. The timing sequence to initiate a drop is given in Table I.

Table I. Sequence of Drop Initiation

Time [s]	Operation	Remarks
- 5	methane valve opens	this allows for the methane to travel to the reaction front
-3	igniter cycle is turned on	fully ignites AP/CH_4 mixture while maintaining ignition wire for pellet retention
-2	visual verification of ignition	verify that the AP is fully ignited and the ignition wire is still entacted
0	drop command	drop command to release Pig Rig package
0 to 5 sec	DAQ recording	all channels recorded at 200 Hz; actual drop occupies 2.2 seconds of recording time

The methane supply was automatically shut-off by a mechanical timer in addition to a software control after 2.2 seconds of drop time, at which time the AP/methane flame extinguished. Below 20 atm, AP does not self deflagrate without an external source of energy, which is provided in the present experiment by the diffusion flame formed between the methane gas and AP decomposition products. Therefore, after the experiment, all of the combustion products were retained in the combustion chamber. After the completion of the experiment, products gases in the sealed Pig Rig were vented through a chemical scrubber prior to exhausting to the environment.

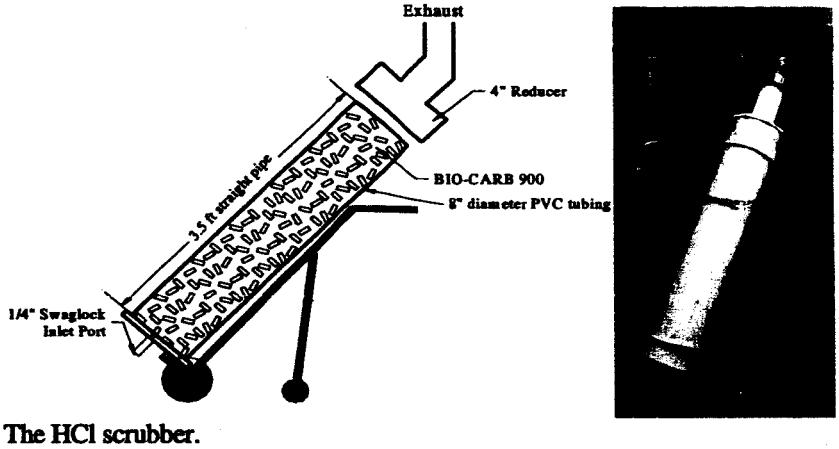

Figure 13. The HCl scrubber.

This project represented a challenge for conducting tests in the drop tower because of safety regulations with regards to the energetic oxidizer and hazardous substances formed during combustion. Prior to conducting experiments, it was important to determine the relative concentrations of the product gases to ensure safe exhausting processes and chamber disassembly since the two major exhaust products of AP and methane combustion are hydrochloric gas (HCl) and water (H_2O). Analytical calculations were performed to conservatively determine the maximum concentrations of each product species as well and the maximum possible chamber pressure were performed to predict extreme conditions of the experiment. The results of these analyses are given in Appendix B. These calculations were used to determine the maximum size of the AP pellet and to design a dry scrubber system for removal of HCl from the trapped test chamber gases after an experiment. The dry scrubber was constructed from PVC pipe and its dimensions are approximately 8 inches in diameter and 42 inches in length to contain the absorbent material (Fig. 13). Activated graphite, BIO-CARB 900, (selected by Richard Caban of MeadWestvaco Air Systems, LLC) was used to remove the HCl. For this absorbent, one gram of HCl consumes approximately seven grams of BIO-CARB 900. For the most extreme test condition, a maximum of 0.23 grams of HCl required scrubbing. Based upon the bulk density of 36 lb/ft^3, there was approximately 16,000 grams of BIO-CARB 900 that was available for reaction with the HCl gas.

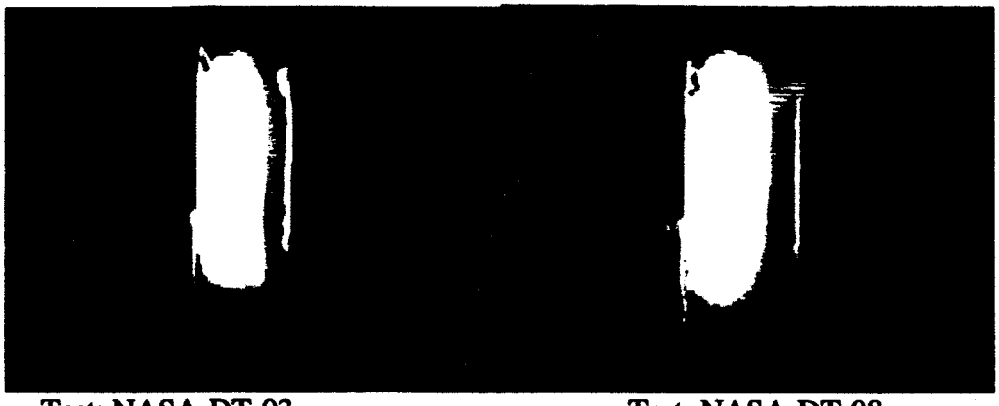

Test: NASA-DT-03 Test: NASA-DT-08

Figure 14. Captured images of the flat flame for two microgravity test runs.

Figure 14 shows a captured image of two separate tests conducted in the 2.2 Second Drop Tower under microgravity conditions. It is apparent that the FSTOP on the lens was set too low for both cases (2.0 and 2.8, respectively).

Figure 15 is the displacement profile of the LVDT for test NASA-DT-03. At 0 seconds, the beginning of the actual drop, the flame had already been established for approximately two seconds. The first slope appears to be 0.104 mm/s, which is in very good agreement with the 1g regression rate data. Immediately after the first slope, there appears to be a rapid increase in burning rate, which then transitions to a slower regression rate. This slower regression rate of 0.051 mm/s is believed to be the microgravity regression rate. The same trend of a rapid acceleration and then reduction in burning rate was also observed in the other successful microgravity experiment that was conducted and appears to indicate the relaxation time for the flame to readjust to microgravity conditions. This time, which is the order of 1 second, is also the same order as characteristic diffusion times for a length scale 5 mm. The drop tower combustion data show that with the same separation distance and flow conditions of the normal gravity experiments, the AP burning rate is approximately a factor of two lower. This difference is likely a result of radiation

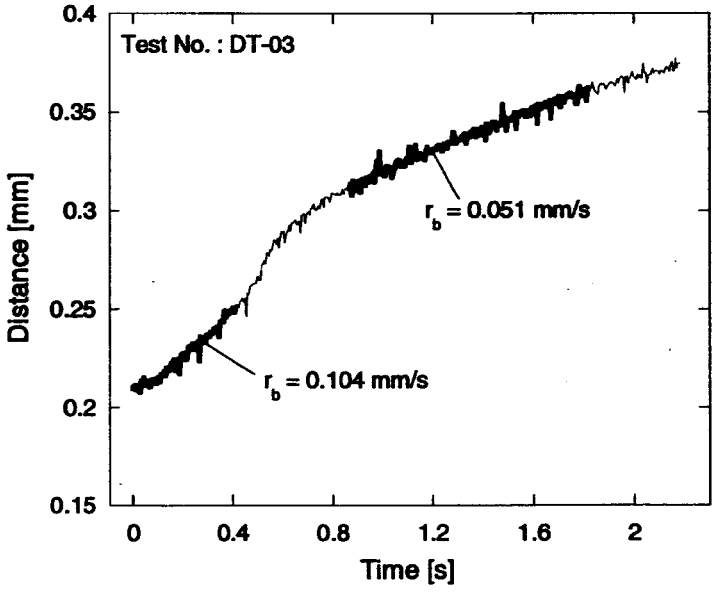

Figure 15. Regression rate data for an AP/CH_4 counterflow experiment in the 2.2s drop tower.

effects, but further tests with longer test times need to be conducted to verify that steady state conditions were achieved under microgravity conditions.

SUMMARY

In this program, counterflow diffusion flames were studied for various fuels flowing against decomposition products from solid AP pellets in order to obtain fundamental understanding of composite propellant flame structure and chemistry. Non-intrusive laser diagnostics measurements were performed to measure a significant number of scalars with which to compare predictions from numerical models. The numerical models were based on detailed reaction mechanisms developed as part of this program. The experiments and modeling calculations were performed using a hierarchical approach starting with simple gaseous fuel systems and proceeding towards more complex systems that are important to binders that are used in practical systems, such as HTPB. The resulting detailed mechanisms form the basis from which reduced mechanisms can be developed for multidimensional modeling calculations of reacting propellant flows. Furthermore, these mechanisms provide the framework for further development of reaction mechanisms for many other propellants, e.g., for those not yet synthesized or formulated. The details of these mechanisms and of the studies on normal gravity counterflow AP flames can be found in our five refereed journal articles and over thirty technical meeting papers and presentations.

Finally, the procedures for conducting combustion experiments with energetic materials in microgravity experiments were also developed. Feasibility experiments were performed in the 2.2s drop tower at NASA Glenn. The initial results obtained from these experiments on AP/CH_4 counterflow flames revealed interesting findings that suggest a reduction in regression rate possibly due to enhanced radiative losses. These results require further study to determine their validity and impact on the AP counterflow flame structure under microgravity conditions. Details of the microgravity tests can be found in unpublished reports [9,10].

ACKNOWLEDGEMENTS

The authors wish to thank Dr. Fumiaki Takahashi and Dr. David Urban for their support as contract monitors of this program. In addition, we also thank Dr. Takahashi for his valuable contributions to the research effort while performing the microgravity combustion experiments at NASA Glenn.

REFERENCES

1. Smooke, M. D., Yetter, R.A., Parr, T. and Hanson-Parr, D., Proc. of the 36th JANNAF Combustion Subcommittee Meeting, Cocoa Beach, FL, (1999).
2. Smooke, M.D., Yetter, R.A., Parr, T.P., Hanson-Parr, D.M., Proceedings of the Combustion Institute, 28, pp. 839-846, (2000).
3. Smooke, M.D., Yetter, R.A., Parr, T.P., Hanson-Parr, D.M., Tanoff, M.A., Colket, M.B., and Hall, R.J., Proceedings of the Combustion Institute, 28, pp. 2013-2020, (2000).
4. Parr, T. P., Hanson-Parr, D.M., Smooke M.D., and Yetter, R.A., Proceedings of the 37th JANNAF Combustion Subcommittee Meeting, Monterey, CA, (2000).
5. Parr, T. P. Hanson-Parr, D.M., Smooke, M.D. and Yetter, R.A., Proceedings of the Combustion Institute, 29, pp. xx-xx, (2002).
6. Parr, T. P., Hanson-Parr, D.M., Smooke M.D., and Yetter, R.A., Proceedings of the Combustion Institute, 30, pp. xx-xx, (2004).
7. Parr, T. P., Hanson-Parr, D. M., "AP Diffusion Flame Structure," 34th JANNAF Combustion Subcommittee Meeting, West Palm Beach, FL, October 1997.
8. Smooke, M. D., McEnally, C. S., Pfefferle, L. D., Hall, R. J. and Colket, M. B., Comb. and Flame, 117, p. 117, (1998).
8. Risha, G., Yetter, R.A., Parr, T.P., Hanson-Parr, D.M., Smooke, M.D., "Safety Permit Request: Study of Energetic Materials in a Counterflow Microgravity Environment," unpublished report, March 2004.
9. Risha, G., Yetter, R.A., Parr, T.P., Hanson-Parr, D.M., Smooke, M.D., "Microgravity Test Results for AP/CH_4 Counterflow Experiments," unpublished report, September 2004.

APPENDIX A: Counterflow Burner Assembly Wiring Diagram

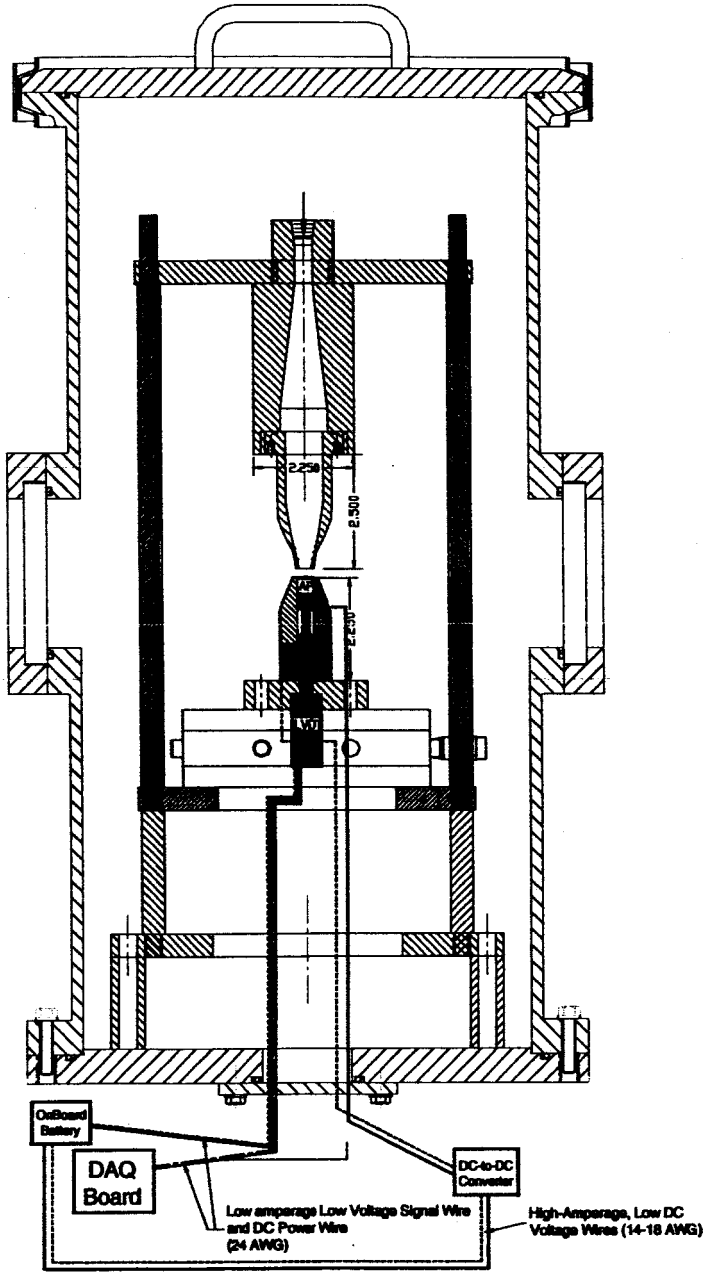

APPENDIX B: Species Concentration Analyses Of Exhaust Products

As mentioned previously, the two major exhaust products of AP and methane combustion are hydrochloric gas (HCl) and water (H_2O). Two approaches (the CEA equilibrium code and an analytical method based upon the change of internal energy) to conservatively determine the maximum concentrations of each product species as well and the maximum possible chamber pressure were performed to predict extreme conditions of the experiment. The results are given in Table B.1.

Table 1. Final products of AP / methane constant volume combustion

Species	CEA (% by vol.) without C(gr) & NH_4Cl(a)		Analytical (% by vol.)		CEA (% by vol.)	
	CASE I	CASE II	CASE I	CASE II	CASE I	CASE II
CH_4	0.517	2.175	0.517	2.182	0.336	1.861
CO	-	-	0.0242	0.1027	-	-
CO_2	0.088	0.380	0.0628	0.267	0.013	0.115
Cl	-	-	0.0141	0.0597	-	-
H	-	-	0.0033	0.0138	-	-
HCl	0.140	0.594	0.125	0.531	-	0.554
H_2	-	0.032	0.0198	0.0839	0.001	0.054
H_2O	0.384	1.617	0.3603	1.531	0.534	2.134
NO	-	-	0.0027	0.0117	-	-
N_2	98.871	95.200	98.839	95.081	98.721	94.677
O	-	-	0.0017	0.0074	-	-
OH	-	-	0.0170	0.0719	-	-
O_2	-	-	0.0127	0.0538	-	-
NH_3	-	-	-	-	-	0.003
C(gr)	-	-	-	-	0.255	0.565
NH_4Cl(a)	-	-	-	-	0.140	0.037
T [K]	327	431	331	432	338	435
P [ATM]	1.063	1.438	1.110	1.452	1.096	1.450

In the first approach, CEA equilibrium calculations were performed under constant volume constant internal energy conditions. In this calculation, all the reactants that were introduced into the test chamber during the prescribed experimental time are instantaneously mixed and are then reacted to achieve full chemical and thermal equilibrium.

In the actual experiment, most of the reaction will take place only in the flame region of the burner, where the products achieve locally high temperatures. These product gases then mix with the remainder of the gas in the test chamber. Since temperatures will drop relatively quickly during the mixing process, it may be assumed that reactions during the mixing and dilution process will be quenched. In order to separate the reaction process from the mixing process, a second "analytical" calculation was performed, in which the total test chamber volume was separated into two sub-volumes. One sub-volume contained the AP and a stoichiometric amount of methane, while the second sub-volume contained the inert nitrogen originally in the test chamber and any excess methane that flows into the container to produce the desired strain rate. After the partial volumes are determined for each of these two sub-volumes, the sub-volume containing the stoichiometric AP and methane is allowed to react at constant volume and constant internal energy to thermal and chemical equilibrium conditions. This sub-volume approximates the high temperature conditions achieved in the flame zone during the experiment. Subsequently, the two sub-volumes are allowed to mix adiabatically without further reaction to achieve thermal equilibrium, but not full chemical equilibrium. In these calculations, the perfect gas law, energy conservation, and ideal gas mixture relations for a closed system are employed.

In both approaches considered, two test durations of 10 and 44 seconds, respectively, were considered. The ten-second test case (CASE I) corresponds to nearly twice the expected actual test duration. The forty-four second test case (CASE II) represents the total time elapsed for a 5-mm long AP pellet to completely burn out. CASE II is the most conservative condition since it corresponds to the case, which the maximum amount of oxidizer is provided to the reactive mixture.

The AP pellet geometry is 10-mm in diameter and 5-mm in length and its burning rate was specified as 0.113 mm/s for both approaches (a value typical of normal gravity conditions). Therefore, it will take 44 seconds for the complete pellet to burn out (provided there exists a constant supply of methane gas in high enough concentration for the 44 seconds), which is 4.4 times the estimated actual total experimental time. For an actual test run, the AP pellet length will be approximately 2.5 mm.

Based upon a test time of 10 seconds, approximately 1-2 mm of the AP pellet will be burned. Assuming a reaction that undergoes a constant volume – constant internal energy process, equilibrium calculations using the NASA CEA code indicate that the test chamber pressure will increase from 1 to 1.063 ATM, while the analytical approach reveals that the pressure will increase to 1.11. A maximum pressure increase of 11% is well within the design specifications of the PIG Rig system. The relative concentrations on a volumetric basis of the CEA code output and analytical equations are shown in Table B.1. Under worst-case test conditions, final mole fractions of 0.00554 HCl and 0.0213 H_2O are predicted. Even under the worst scenario of an uncontrolled burn to completion, the chamber pressure is predicted to rise to approximately 1.45 ATM, which again is well within the safety margins of the PIG Rigs. For these full equilibrium calculations using the entire CEA species database, some carbon graphite and $NH_4Cl(a)$ are predicted to form as equilibrium species. Assuming that insufficient time is available to form these two species

because of the low temperatures, they were omitted from the database and the calculations were repeated. As seen in Table 1 (columns 3 and 4), some redistribution of the equilibrium species is predicted.

The analytical approach comprised of a sequential process. In this discussion, since the methodology for both reaction time cases is identical, only CASE I will be described here. The amount of the fuel (methane) and oxidizer (AP) to burn stoichiometrically was determined on a mass basis. On a stoichiometric molar basis, 1 mole of CH_4 reacts with 1.6 moles AP. Assuming that the AP pellet burns at 0.113 mm/s, the length of the AP pellet burned is

$$L_{burned} = r_{b,AP}\Delta t = \left(0.0113\,\frac{cm}{s}\right)(10\ s) \Rightarrow L_{burned} = 0.113\ cm \qquad \text{Eq. (B.1)}$$

Therefore, the volume amount of the burned AP pellet is given by

$$\forall_{AP} = \frac{\pi D_{AP}^2}{4} L_{burned} = \frac{\pi(1\ cm)^2}{4}(0.113\ cm) \Rightarrow \forall_{AP} = 0.08875\ \ cm^3 \qquad \text{Eq. (B.2)}$$

Using the volume determined from Eq. (B.2), the mass of AP pellet can be calculated as

$$m_{AP} = \forall_{AP}\rho_{AP} = (0.08875\ cm^3)\left(1.95\,\frac{gm}{cm^3}\right) \Rightarrow m_{AP} = 0.1731\ gm \qquad \text{Eq. (B.3)}$$

Therefore, the number of moles of AP is NAP = 0.00148 moles.

For stoichiometric conditions on a molar basis, the number of required methane moles is determined as

$$\frac{N_{AP}}{N_{CH4}} = 1.6 \Rightarrow N_{CH4} = \frac{N_{AP}}{1.6} = \frac{0.00148}{1.6} \Rightarrow N_{CH4} = 0.000924\ \ moles \qquad \text{Eq. (B.4)}$$

Converting moles of CH_4 to grams of CH_4, yields

$$m_{CH4} = N_{CH4} MW_{CH4} = 0.000924\ moles\left(16\,\frac{gm}{mole}\right) \Rightarrow m_{CH4} = 0.0148\ \ gm \qquad \text{Eq. (B.5)}$$

The volume, which the reactants occupied in the test chamber, was approximated using the ideal gas law in order to obtain input data for a constant volume-constant internal energy calculation with the CEA code. The volume occupied by CH_4 is

$$\forall_{CH4} = \frac{m_{CH4} R T_{CH4}}{P_{CH4}} = \frac{(0.0000148\ kg)\left(\frac{8315\ J/kmol-K}{16\ kg/kmol}\right)(300\ K)}{102035\,\frac{N}{m^2}} \qquad \text{Eq. (B.6)}$$

$$\forall_{CH4} = 0.00022613\ \ m^3 = 22.61\ cm^3$$

Similarly, the volume of AP is $\forall_{AP} = 8.87 \times 10^{-8}\ m^3 = 0.0887\ cm^3$. Thus, the volume occupied by both of the reactants is given as

$$\forall_{reac} = \forall_{CH4} + \forall_{AP} = 22.61\ cm^3 + 0.0887\ cm^3 \Rightarrow \forall_{reac} = 22.699\ \ cm^3 \qquad \text{Eq. (B.7)}$$

Finally, the loading density input parameter for CEA is given as

$$\rho_{reac} = \frac{m_{AP} + m_{CH4}}{V_{reac}} = \frac{0.0148\,gm + 0.1731\,gm}{22.699\,cm^3} \Rightarrow \rho_{reac} = 0.00828\,\frac{gm}{cm^3} \qquad \text{Eq. (B.8)}$$

Using the previously-calculated amount of reactive ingredients and the loading density as input data to the UV problem in CEA, the maximum equilibrium pressure and temperature was calculated to be

PMAX = 79.91 ATM and TMAX = 2971 K

The final step of the analytical method was to mix the hot product gases with the cold atmospheric gases. The cold gases consist of 1.046 moles of nitrogen and 0.005475 moles of excess CH_4. The first law of thermodynamics for a closed system can be used to determined the final mixture temperature and is given as

$$\Delta E = Q - W = \Delta PE + \Delta KE + \Delta U = Q - W \qquad \text{Eq. (B.9)}$$

Assuming no heat loss, no work, and the change in potential and kinetic energies are negligible, the expression for the change in internal energy is given as

$$\Delta U = 0 \qquad \text{Eq. (B.10)}$$

Therefore,

$$U_2(T_f) = U_1(T_{1,N2}, T_{1,CH4,excess}, T_{1,prod})$$

We know that U1 in Eq. (B.11a) represents the sum of the internal energies of the gases at their respective initial state, while U2 in Eq. (B.11b) represents the internal energy of the mixture at its final temperature, T_f. The species considered in Eq. (B.10) were CH_4, CO, CO_2, Cl, H, HCl, H_2, H_2O, NO, N_2, O, OH, and O_2, resulting in

$$U1 = 7343\ J \qquad \text{Eq. (B.11a)}$$

$$U2 = 22.18(Tf)\ J/K \qquad \text{Eq. (B.11b)}$$

Solving the ratio of Eqs. (B.11a) and (B.11b) for T_f,

$$T_f = \frac{7343\,J}{22.18\,J/K} \Rightarrow T_f = 331\,K$$

Note: CEA equilibrium result was 327 K

To determine pressure, we know that the total volume of the chamber can be defined as

$$V_{final} = V_{CH4,excess} + V_{prod} + V_{N2} \qquad \text{Eq. (B.12)}$$

Substituting the ideal gas law in Eq. (B.12), we obtain the following expression for P_f

$$P_f = \frac{(n_{prod} + n_{CH4,excess} + n_{N2}) \cdot T_f}{\frac{n_{prod} T_{prod}}{P_{prod}} + \frac{T_{CH4,excess}}{P_{CH4,excess}}(n_{CH4,excess} + n_{N2})} \qquad \text{Eq. (B.13)}$$

$$P_f = 1.1103\ ATM$$

Note: CEA equilibrium result was 1.063 ATM

The results of this calculation that were shown in Table B.1 are in good agreement with the full CEA equilibrium calculation when C(gr) and NH_4Cl(a) are omitted from the database.

APPENDIX C: Chamber Surface Temperature Estimation

The results of CASE II will be used to determine the maximum chamber surface temperature for the most extreme condition. In the calculation described below, the estimated change in chamber temperature for the most extreme case experiment was found to be $\Delta T = 0.23$ K. The touch temperature of the chamber outer wall must be less than 49°C. The products species and moles are listed in Table C.1.

Table C.1. Final products of AP / methane constant volume combustion

Species	CASE II (vol%)	Moles
CH_4	1.861	0.02077
CO	-	-
CO_2	0.115	0.001283
Cl	-	-
H	-	-
HCl	0.554	0.006182
H_2	0.054	0.000603
H_2O	2.134	0.023813
NO	-	-
N_2	94.677	1.0565
O	-	-
OH	-	-
O_2	-	-
NH_3	0.003	0.0000335
C(gr)	0.565	0.006305
$NH_4Cl(a)$	0.037	0.000413

The energy delivered to the chamber can be determined by

$$q = m_{cham} \cdot C_{cham} \cdot \Delta T \qquad \text{Eq. (C.1)}$$

Given Information:

$m_{cham} = 22$ kg

$C_{cham} = 0.21$ kcal/mol

The heat of combustion for reactants and products at ambient temperature (Tref=298.15 K) can be written as

$$\Delta H_{comb\,@\,298K} = (H_{prod} - H_{reac})_{@\,298K} \qquad \text{Eq. (C.2)}$$

Therefore, the chemical energy is given by

$$\Delta H_{comb\,@\,298K} = \sum_{reactants} n_i \Delta H^{\circ}_{f,i} - \sum_{products} n_i \Delta H^{\circ}_{f,i} \qquad \text{Eq. (C.3)}$$

Assuming the energy generated from the combustion process can be delivered to the chamber walls, we can say

$$\Delta H_{comb\,@\,298K} = q = m_{cham} \cdot C_{Alum} \cdot \Delta T \qquad \text{Eq. (C.4)}$$

Thus, solving for the final wall temperature, we get

$$\Delta T = T_f - T_i = \frac{\Delta H_{comb\,@\,298K}}{m_{cham} \cdot C_{Alum}} \quad \Rightarrow \quad T_f = \frac{\Delta H_{comb\,@\,298K}}{m_{cham} \cdot C_{Alum}} + T_i \qquad \text{Eq. (C.5)}$$

Inserting the results tabulated in Table C.1 into Eq. (C.3), the heat of combustion can be determined as

$$\Delta H_{comb\,@\,298K} = \left[\begin{matrix} n_{CH4}\Delta H^{\circ}_{f,CH4} + n_{AP}\Delta H^{\circ}_{f,AP} \\ + n_{N2}\Delta H^{\circ}_{f,N2} \end{matrix} \right]_{REAC} - \left[\begin{matrix} n_{CH4}\Delta H^{\circ}_{f,CH4} + n_{CO2}\Delta H^{\circ}_{f,CO2} + n_{HCl}\Delta H^{\circ}_{f,HCl} \\ + n_{H2}\Delta H^{\circ}_{f,H2} + n_{H2O}\Delta H^{\circ}_{f,H2O} + n_{N2}\Delta H^{\circ}_{f,N2} \\ + n_{NH3}\Delta H^{\circ}_{f,NH3} + n_{C(gr)}\Delta H^{\circ}_{f,C(gr)} + n_{NH4Cl}\Delta H^{\circ}_{f,NH4Cl} \end{matrix} \right]_{PROD}$$

$$\Delta H_{comb\,@\,298K} = -4.046\,\text{kJ} - (-8.521\,\text{kJ})$$

$$\Delta H_{comb\,@\,298K} = 4.475\,\text{kJ}$$

Now, substitute the heat of combustion into Eq. (C.5), we have

$$T_f = \frac{4.475\,\text{kJ}/\text{mol}}{22\,\text{kg} \cdot 0.21\,\text{kcal}/\text{mol} - \text{K} \cdot \left(\frac{4.1868\,\text{kJ}}{\text{kcal}} \right)} + 298.15\,\text{K}$$

$$T_f = 0.2313\,\text{K} + 298.15\,\text{K} \quad \Rightarrow \quad T_f = 298.38\,\text{K} \quad << \quad 322.15\,\text{K}$$